JOURNAL OF SOLID STATE CHEMISTRY **130,** 9–19 (1997)
ARTICLE NO. SC977252

A New Structural Family: $M_{10n-2}Ge_{3n+1}O_{16n}$ with M = (Co, Mg) and (Ni, Mg)

David Lévy and Jacques Barbier[1]

Department of Chemistry, McMaster University, Hamilton, Ontario L8S 4M1, Canada

Received August 26, 1996; accepted November 27, 1996

The structures of three new germanates have been determined by single-crystal X-ray diffraction: $(Co_{0.62}Mg_{0.38})_{24}Ge_8O_{40}$, orthorhombic *Pnma*, $a = 10.193(2)$, $b = 5.941(1)$, $c = 24.200(5)$ Å, $Z = 2$, $wR(F^2) = 0.080$ for all 3480 independent reflections; $(Co_{0.52}Mg_{0.48})_{14}Ge_5O_{24}$, orthorhombic *Pbam*, $a = 14.537(3)$, $b = 10.219(2)$, $c = 5.950(1)$ Å, $Z = 2$, $wR(F^2) = 0.082$ for all 2942 independent reflections; $(Ni_{0.21}Mg_{0.79})_{14}Ge_5O_{24}$, orthorhombic *Pbam*, $a = 14.446(3)$, $b = 10.174(2)$, $c = 5.917(1)$ Å, $Z = 2$, $wR(F^2) = 0.079$ for all 2789 independent reflections. The latter two compounds are isostructural with the previously known $Mg_{14}Ge_5O_{24}$ germanate. The $M_{24}Ge_8O_{40}$ and $M_{14}Ge_5O_{24}$ structures represent the members $n = 5$ and $n = 3$, respectively, of a new structural family, $M_{10n-2}Ge_{3n+1}O_{16n}$ with M = (Co, Mg) or (Ni, Mg). The $n = \infty$ end member of this series corresponds to the $M_{10}Ge_3O_{16}$ structure previously characterized in the CoO/NiO–MgO–GeO_2 systems, and the other $n = 1$ end member corresponds to the well-known M_2GeO_4 olivine structure. The structural family is based on the building principle of unit-cell twinning: the nth member is obtained by the periodic insertion of glide planes on every nth (011) plane of the rhombohedral $M_{10}Ge_3O_{16}$ end member. As expected, transmission electron microscopy has revealed the common occurrence of intergrowths in multiphase samples. © 1997 Academic Press

INTRODUCTION

The original study of phase relations in the NiO–MgO–GeO_2 and CoO–MgO–GeO_2 systems (1) established the similarity between them, as well as the existence in the cobalt system of phases possibly structurally related to the previously known $Mg_{14}Ge_5O_{24}$ compound (2). Later, a reinvestigation of the nickel system led to the structure determination of a new germanate, $(Ni, Mg)_{10}Ge_3O_{16}$ (3–5), and its description as a member of a new structural family formulated then as $M_{4n+6}Ge_{2n+1}O_{8(n+1)}$ (6). The simultaneous presence of tetrahedrally and octahedrally coordinated Ge atoms in these compounds led to the speculation that silicate analogs might form under high-pressure conditions. This suggestion was indeed confirmed afterward by the syntheses of the $Mg_{14}Si_5O_{24}$ and $(Fe, Mg)_{14}Si_5O_{24}$ compounds at very high pressures and temperatures (e.g., 16 GPa, 2400°C) and their structure determinations by single-crystal X-ray diffraction (7–9).

Recently, a new study of the CoO–MgO–GeO_2 system was undertaken in order to clarify the nature of the unidentified phases reported in the original work (1). Initial results led to the structure determination of a new cobalt germanate, $Co_{10}Ge_3O_{16}$ (10), isostructural with $(Ni, Mg)_{10}Ge_3O_{16}$ (referred to as the M_{10} phase hereafter). Further work has now resulted in the synthesis of two other phases, $(Co, Mg)_{24}Ge_8O_{40}$ and $(Co, Mg)_{14}Ge_5O_{24}$ (denoted M_{24} and M_{14}, respectively), the crystal structures of which are reported in the present paper, along with that of the $(Ni, Mg)_{14}Ge_5O_{24}$ phase. The structure determination of the new M_{24} phase, which was unknown at the time of the previous study of the NiO–MgO–GeO_2 system (6), shows that the structural family formed by the M_{10}, M_{24}, and M_{14} phases must now be reformulated as $M_{10n-2}Ge_{3n+1}O_{16n}$. Its building principle is also described in this paper.

EXPERIMENTAL

Powder Work

The phase relations in the CoO–MgO–GeO_2 system were initially investigated by X-ray diffraction on microcrystalline powders. In all cases, the compounds were synthesized from stoichiometric mixtures of high-purity (99% or better) powders of MgO, $CoCO_3$, and GeO_2 which were mixed thoroughly, pressed into pellets of 0.5 g each and fired at temperatures of 1000–1200°C for several days with intermediate remixings. The reaction products were then characterized with a Guinier–Lenné camera using Fe$K\alpha_1$ radiation in order to avoid the strong fluorescence due to cobalt in the presence of Cu radiation.

The results of this work are summarized in Fig. 1 which shows the locations of the three compounds $M_{10}Ge_3O_{16}$, $M_{24}Ge_8O_{40}$, and $M_{14}Ge_5O_{24}$ (M = Co, Mg). Due to the

[1] To whom correspondence should be addressed.

0022-4596/97 $25.00
Copyright © 1997 by Academic Press
All rights of reproduction in any form reserved.

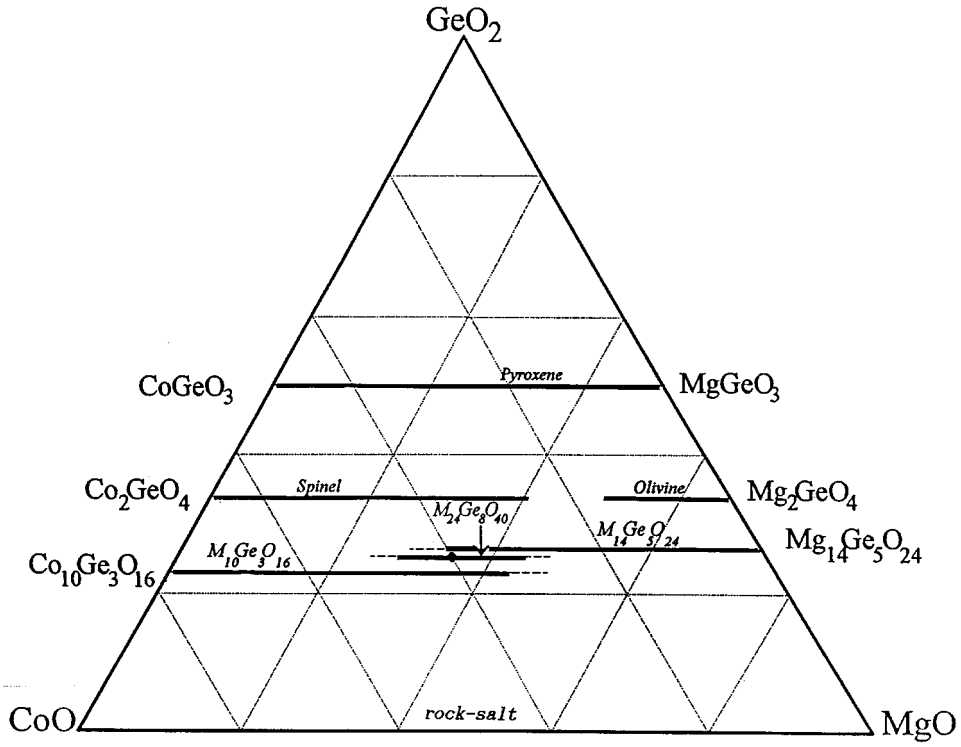

FIG. 1. Phase diagram of the CoO–MgO–GeO_2 system showing the approximate composition ranges of the $M_{10n-2}Ge_{3n+1}O_{16n}$ phases at temperatures between 1000 and 1200°C. The pyroxene, spinel, olivine, and rock-salt solid solutions are taken from Ref. 1.

close proximity of their chemical compositions (in terms of M/Ge ratios), it proved difficult to synthesize truly single-phase samples in the central region of the phase diagram and the limits of the solid solutions could only be determined approximately. It is noteworthy that, whereas the M_{24} and M_{14} phases were found to be stable at the highest temperature used (i.e., 1200°C), the M_{10} phase was observed to become markedly less stable with an increasing Mg/Co ratio: for instance, the $Co_{10}Ge_3O_{16}$ compound melts congruently around 1250°C (10), but the $Co_6Mg_4Ge_3O_{16}$ phase decomposes completely without melting into a mixture of the M_{24} and (Co, Mg)O phases when heated to 1200°C for 12 hr. It was, in fact, this solid-state decomposition reaction which initially led to the identification of the new M_{24} phase. It is also worth emphasizing that, in the phase diagram of Fig. 1, the M_{24} phase forms at intermediate compositions (in terms of (Co + Mg)/Ge ratios) between those of the M_{10} and M_{14} phases. As shown further below from the results of the structure determinations, this compositional relationship correlates very well with the structural relationship existing among these three phases.

Crystal Growth

The experimental conditions that yielded the best crystals of each phase are listed in Table 1. Single crystals of the M_{24} and M_{14} phases in the CoO–MgO–GeO_2 system were grown from a K_2MoO_4 flux. Due to the close proximity of these two phases in the phase diagram (cf. Fig. 1), the same starting material was used as nutrient for the crystal growth experiments, i.e., a powder with a nominal composition of 40% CoO–35% MgO–25% GeO_2 (in mole%) prereacted for 3 days at 1200°C. However, it was found that the growth of crystals of the M_{24} phase was enhanced by the addition of a cobalt excess to the melt (cf. Table 1). Single crystals of the M_{14} phase in the NiO–MgO–GeO_2 system were also grown

TABLE 1
Experimental Conditions for the Flux Growth of Single Crystals of the $(Co, Mg)_{24}Ge_8O_{40}$, $(Co, Mg)_{14}Ge_5O_{24}$, and $(Ni, Mg)_{14}Ge_5O_{24}$ Compounds

	M_{24}(Co)	M_{14}(Co)	M_{14}(Ni)
K_2MoO_4 flux (g)	20.3	20.3	24
Nutrient (g)	0.5	1.5	1.5
(see text)	(+ 0.2 g $CoCO_3$)		
Soaking conditions	24 hr	12 hr	10 hr
	at 1250°C	at 1250°C	at 1250°C
Cooling conditions	2°C/hr	1°C/hr	2°C/hr
	to 1050°C	to 1150°C	to 1000°C
Crystal morphology	Pink plates (twinned arrowheads)	Pink prisms	Green rods

from a K_2MoO_4 flux with a nutrient of composition 27% NiO–47% MgO–26% GeO_2 (in mole%). For each phase, a crystal of suitable quality for the collection of X-ray intensity data was selected by examination with an optical microscope and a precession camera.

Structure Determinations

The details of the crystal data, data collections, and structure refinements for the $(Co, Mg)_{24}Ge_8O_{40}$, $(Co, Mg)_{14}Ge_5O_{24}$, and $(Ni, Mg)_{14}Ge_5O_{24}$ phases are listed in Tables 2, 3, and 4, respectively. Prior to the structure determinations, all three data sets were corrected for absorption effects using the XPREP routine of the SHELXL software (11). In the case of $(Co, Mg)_{24}Ge_8O_{40}$, an untwinned fragment was cut from a twinned crystal and its shape was approximated as a (001) plate bounded by ($\pm$100), ($\pm$010), (110), and (2–10) faces. The crystal selected for $(Co,Mg)_{14}Ge_5O_{24}$ was an untwinned rectangular prism bounded by ($\pm$100), ($\pm$010), and ($\pm$001) faces, flattened along the *a* direction. The $(Ni, Mg)_{14}Ge_5O_{24}$ crystals were obtained as thin rod-like prisms elongated along the *c* axis and, in this case, psi-scan data were used for the absorption correction.

In all three cases, the structure was solved by a combination of direct methods and Fourier syntheses using the SHELXS (12) and SHELXL (11) softwares. Although no chemical analyses of the crystals have been carried out, the Co/Mg and Ni/Mg ratios were unambiguously determined as part of the structure refinements as follows: in a first

TABLE 2
Single-Crystal X-Ray Data Collection and Refinement of $(Co, Mg)_{24}Ge_8O_{40}$

Crystal data			
Chemical formula			$Co_{14.9}Mg_{9.1}Ge_8O_{40}$
Crystal system			Orthorhombic
Space group			*Pnma*
Z			2
a (Å)			10.193(2)
b (Å)			5.941(1)
c (Å)			24.200(5)
V (Å^3)			1465.5
D_x (Mg m^{-3})			5.23
Radiation			Mo$K\alpha$
Wavelength (A)			0.71073
Absorption coefficient			16.38 mm^{-1}
Temperature (K)			Room temperature
Description			Dark pink (001) plate
Size (mm)			$0.25 \times 0.12 \times 0.03$ (see text)
Data collection			
Diffractometer type			Siemens P4, rotating anode
Collection method			2θ–θ
2θ max (deg)			70
h_{min}	-1	h_{max}	16
k_{min}	-1	k_{max}	9
l_{min}	-39	l_{max}	1
No. of reflections measured			4760
No. of standard reflections			3 every 100 (no decay)
No. of observed reflections			4492 ($I > 3\ \sigma(I)$)
Absorption correction			Gaussian face-indexed (see text)
			$T_{min} = 0.197$ $T_{max} = 0.613$
No. of independent reflections			3480 ($R_{int} = 0.040$)
Refinement (on F^2)			
No. of parameters refined			194
No. of reflections used			3480
Weighting scheme			$w = [\sigma^2(F_o^2) + (0.0345\,P)^2]^{-1}$
			where $P = (\max(F_o^2, 0) + 2F_c^2)/3$
Extinction correction			$[1 + 0.001\ (c)\ F_c^2\ \lambda^3/\sin 2\theta]^{-1/4}$
Extinction parameter			$c = 0.0012(1)$
Atomic scattering factors			Neutral atoms from SHELXL software
$R1(F)$	0.031 for 2808 $F_o > 4\sigma(F_o)$	$(\Delta/\sigma)_{max}$	0.001
$R1(F)$	0.045 for all 3480 data	$(\Delta\rho)_{min}$ (e·Å^{-3})	-1.1
$wR2(F^2)$	0.080 for all 3480 data	$(\Delta\rho)_{max}$ (e·Å^{-3})	1.6
S	1.102		

TABLE 3
Single-Crystal X-Ray Data Collection and Refinement of $(Co, Mg)_{14}Ge_5O_{24}$

Crystal data			
Chemical formula			$Co_{7.3}Mg_{6.7}Ge_5O_{24}$
Crystal system			Orthorhombic
Space group			*Pbam*
Z			2
a (Å)			14.537(3)
b (Å)			10.219(2)
c (Å)			5.950(1)
V (Å^3)			883.9
D_x (Mg m^{-3})			5.03
Radiation			Mo$K\alpha$
Wavelength (A)			0.71073
Absorption coefficient			15.36 mm^{-1}
Temperature (K)			Room temperature
Description			Dark pink flat prism
Size (mm)			$0.18 \times 0.18 \times 0.08$ (see text)
Data collection			
Diffractometer type			Siemens P4, rotating anode
Collection method			2θ–θ
2θ max (deg)			80
h_{min}	0	h_{max}	26
k_{min}	0	k_{max}	18
l_{min}	-10	l_{max}	0
No. of reflections measured			3141
No. of standard reflections			3 every 100 (no decay)
No. of observed reflections			2942 ($I > 3\ \sigma(I)$)
Absorption correction			Gaussian face-indexed (see text)
			$T_{min} = 0.093$ $T_{max} = 0.310$
No. of independent reflections			2942 (R_{int} = N/A)
Refinement (on F^2)			
No. of parameters refined			119
No. of reflections used			2942
Weighting scheme			$w = [\sigma^2(F_o^2) + (0.0397\,P)^2]^{-1}$
			where $P = (\max(F_o^2, 0) + 2F_c^2)/3$
Extinction correction			$[1 + 0.001\ (c)\ F_c^2\ \lambda^3/\sin 2\theta]^{-1/4}$
Extinction parameter			$c = 0.0166(5)$
Atomic scattering factors			Neutral atoms from SHELXL software
$R1(F)$	0.031 for 2533 $F_o > 4\ \sigma(F_o)$	$(\Delta/\sigma)_{max}$	0.001
$R1(F)$	0.039 for all 2942 data	$(\Delta\rho)_{min}$ (e·Å^{-3})	-1.2
$wR2(F^2)$	0.082 for all 2942 data	$(\Delta\rho)_{max}$ (e·Å^{-3})	1.5
S	1.11		

TABLE 4
Single-Crystal X-Ray Data Collection and Refinement of $(Ni, Mg)_{14}Ge_5O_{24}$

Crystal data			
Chemical formula			$Ni_{2.9}Mg_{11.1}Ge_5O_{24}$
Crystal system			Orthorhombic
Space group			*Pbam*
Z			2
a (Å)			14.446(3)
b (Å)			10.174(2)
c (Å)			5.917(1)
V (Å^3)			869.6
D_x (Mg m^{-3})			4.55
Radiation			Ag$K\alpha$
Wavelength (A)			0.56086
Absorption coefficient			6.41 mm^{-1}
Temperature (K)			Room temperature
Description			Green rod-like prism
Size (mm)			$0.3 \times 0.02 \times 0.02$
Data collection			
Diffractometer type			Siemens R3m/v
Collection method			2θ–θ
$2\theta_{max}$ (deg)			60
h_{min}	-1	h_{max}	25
k_{min}	-1	k_{max}	18
l_{min}	-1	l_{max}	10
No. of reflections measured			3824
No. of standard reflections			3 every 100 (no decay)
No. of observed reflections			3586 ($I > 3\ \sigma(I)$)
Absorption correction			Psi-scan
			$T_{min} = 0.382$ $T_{max} = 0.488$
No. of independent reflections			2789 ($R_{int} = 0.059$)
Refinement (on F^2)			
No. of parameters refined			119
No. of reflections used			2789
Weighting scheme			$w = [\sigma^2(F_o^2) + (0.0202\ P)^2]^{-1}$ where $P = (\max(F_o^2, 0) + 2\ F_c^2)/3$
Extinction correction			$[1 + 0.001\ (c)\ F_c^2\ \lambda^3/\sin 2\theta]^{-1/4}$
Extinction parameter			$c = 0.0071(3)$
Atomic scattering factors			Neutral atoms from SHELXL software
$R1(F)$	0.042 for 1414 $F_o > 4\ \sigma(F_o)$	$(\Delta/\sigma)_{max}$	0.000
$R1(F)$	0.103 for all 2789 data	$(\Delta\rho)_{min}$ (e·Å^{-3})	-1.6
$wR2(F^2)$	0.079 for all 2789 data	$(\Delta\rho)_{max}$ (e·Å^{-3})	1.3
S	0.75		

stage, the isotropic displacement parameters (U_{eq}) of the metal octahedral sites were constrained to be equal while the individual site occupancies were refined (yielding e.s.d.'s of 0.5% or better for all sites). In a second stage, these occupancies were fixed at their refined values and the individual U_{eq} parameters were allowed to vary independently. Finally, fully anisotropic models were refined, converging smoothly to the reliability indices listed in Tables 2, 3, and 4. The final atomic coordinates, equivalent displacement parameters, and site occupancies for the $(Co, Mg)_{24}Ge_8O_{40}$, $(Co, Mg)_{14}Ge_5O_{24}$, and $(Ni, Mg)_{14}Ge_5O_{24}$ structures are given in Tables 5, 6, and 7, respectively. Tables of anisotropic displacement parameters are available from the authors upon request.

TABLE 5
Atomic Coordinates [$\times 10^4$], Equivalent Isotropic Displacement Parameters [$\times 10^4$] and Site Occupancies (%Mg = 100–%Co) for $(Co, Mg)_{24}Ge_8O_{40}$

	x	y	z	U_{eq} (Å^2)	%Co ($\pm$ 0.5)
Ge(1)	5809(1)	2500	3257(1)	35(1)	
Ge(2)	4130(1)	7500	5236(1)	34(1)	
Ge(3)	7598(1)	7500	2886(1)	44(1)	
Ge(4)	831(1)	2500	3982(1)	33(1)	
M(1)	2557(1)	2500	4977(1)	50(1)	69.3
M(2)	9066(1)	2500	2940(1)	53(2)	31.0
M(3)	6669(1)	55(1)	2018(1)	51(1)	72.0
M(4)	5622(1)	2500	7030(1)	53(2)	41.6
M(5)	840(1)	7500	3982(1)	50(1)	87.1
M(6)	3381(1)	36(1)	3998(1)	49(1)	66.8
M(7)	0	0	5000	48(2)	80.9
M(8)	8306(1)	111(1)	4013(1)	50(2)	53.1
M(9)	5813(1)	7500	4039(1)	52(2)	49.3
O(1)	5795(3)	2500	2525(1)	52(5)	
O(2)	5038(2)	15(3)	3499(1)	60(4)	
O(3)	4161(2)	7500	4505(1)	50(5)	
O(4)	3329(2)	9947(3)	5476(1)	56(4)	
O(5)	8340(2)	9763(4)	2546(1)	61(4)	
O(6)	61(2)	277(3)	3534(1)	55(4)	
O(7)	7517(3)	7500	3593(1)	54(5)	
O(8)	2353(3)	2500	3531(1)	56(5)	
O(9)	2565(2)	7500	3487(1)	57(5)	
O(10)	3933(2)	2500	7452(1)	53(5)	
O(11)	853(2)	2500	5490(1)	60(5)	
O(12)	-669(2)	2500	4446(1)	45(5)	
O(13)	7458(2)	2500	3488(1)	51(5)	
O(14)	5759(2)	7500	5498(1)	55(5)	
O(15)	1601(2)	266(3)	4434(1)	51(4)	

DESCRIPTION OF THE CRYSTAL STRUCTURES

The $(Co, Mg)_{24}Ge_8O_{40}$ Phase

The crystal structure of this new phase is depicted in Fig. 2 and the corresponding bond distances are listed in Table 8. (A table of bond angles is available from the authors upon request). The structure is based on a mixed cubic–hexagonal close-packing of oxygen atoms with a ten-layer (c^4hc^4h) repeat along the c axis. The Ge atoms occupy both tetrahedral (Ge1, Ge2, and Ge3) and octahedral (Ge4) sites whereas the Co and Mg atoms are found with mixed occupancies in octahedral sites only. The location of the hexagonal (h) layers at $z = \pm 1/4$ within the unit cell corresponds to the presence of the glide planes in the *Pnma* space group. These (h) layers result in the formation of olivine-type (001) slabs (containing the $M2$, $M3$, $M4$, Ge1, and Ge3 sites—cf. Fig. 2) and their periodic distribution corresponds to the glide-reflection twinning operation (13) used to generate the $M_{10n-2}Ge_{3n+1}O_{16n}$ structural family (cf. last section below).

TABLE 6
Atomic Coordinates [×10⁴], Equivalent Isotropic Displacement Parameters [×10⁴] and Site Occupancies (%Mg = 100−%Co) for $(Co, Mg)_{14}Ge_5O_{24}$

	x	y	z	U_{eq} (Å²)	%Co (± 0.5)
Ge(1)	0	0	0	37(1)	
Ge(2)	1256(1)	5016(1)	0	36(1)	
Ge(3)	1860(1)	3238(1)	5000	44(1)	
M(1)	0	5000	5000	53(2)	34.2
M(2)	0	0	5000	53(2)	89.8
M(3)	1749(1)	1777(1)	0	53(1)	25.8
M(4)	3269(1)	1469(1)	5000	55(1)	38.3
M(5)	− 44(1)	2522(1)	2406(1)	52(1)	51.7
M(6)	3309(1)	4186(1)	2457(1)	52(1)	66.6
O(1)	844(1)	3380(2)	0	59(3)	
O(2)	4221(1)	3496(2)	0	52(3)	
O(3)	2524(1)	38(2)	0	55(3)	
O(4)	680(1)	3301(2)	5000	54(3)	
O(5)	4127(1)	3300(2)	5000	55(3)	
O(6)	2579(1)	− 233(2)	5000	59(3)	
O(7)	751(1)	779(1)	2220(2)	54(3)	
O(8)	4141(1)	803(1)	2472(2)	56(3)	
O(9)	2420(1)	2498(1)	2730(3)	60(3)	

As seen in Table 5, a significant Co/Mg ordering is observed in the $(Co, Mg)_{24}Ge_8O_{40}$ structure with Co contents that range from 31% in the *M*2 site to 87% in the *M*5 site, for an overall composition of 62% Co. Interestingly, there is a complete lack of correlation between the average *M*–O distances (cf. Table 8) and the site populations which indicates that the octahedral coordination geometries are predominantly determined by the pattern of edge-sharing and the associated atomic shifts within the structure. It is noteworthy, however, that the highest Co contents occur at the *M*5 and *M*7 sites which both share two opposite edges with the $Ge4O_6$ octahedron (cf. Fig. 2), and that the lowest Co contents are found for the most irregular *M*2 and *M*4 sites (i.e., with the widest spread of *M*–O distances). A similar trend is also observed in the $(Co, Mg)_{14}Ge_5O_{24}$ structure and is discussed further below.

TABLE 7
Atomic coordinates [×10⁴], Equivalent Isotropic Displacement Parameters [×10⁴] and Site Occupancies (%Mg = 100−%Ni) for $(Ni, Mg)_{14}Ge_5O_{24}$

	x	y	z	U_{eq} (Å²)	%Ni (± 0.5)
Ge(1)	0	0	0	47(2)	
Ge(2)	1257(1)	5017(1)	0	52(1)	
Ge(3)	1865(1)	3253(1)	5000	61(1)	
M(1)	0	5000	5000	58(4)	16.4
M(2)	0	0	5000	62(2)	58.0
M(3)	1761(1)	1783(2)	0	62(4)	1.8
M(4)	3265(1)	1476(2)	5000	64(3)	9.8
M(5)	− 43(1)	2515(1)	2417(2)	62(2)	23.6
M(6)	3315(1)	4189(1)	2459(2)	62(2)	27.1
O(1)	841(3)	3378(4)	0	53(7)	
O(2)	4224(3)	3483(4)	0	63(8)	
O(3)	2515(2)	37(4)	0	74(7)	
O(4)	675(2)	3298(4)	5000	65(8)	
O(5)	4136(3)	3309(4)	5000	64(7)	
O(6)	2560(3)	− 222(4)	5000	83(8)	
O(7)	750(2)	774(2)	2238(5)	69(5)	
O(8)	4140(2)	806(2)	2471(5)	59(5)	
O(9)	2432(2)	2515(3)	2730(5)	73(5)	

The $(Co, Mg)_{14}Ge_5O_{24}$ and $(Ni, Mg)_{14}Ge_5O_{24}$ Phases

As noted earlier, these phases are isostructural with the $Mg_{14}Ge_5O_{24}$ compound (2). The crystal structure of the cobalt phase is depicted in Fig. 3 and the associated bond distances are given in Table 9. Bond distances for the nickel phase are listed in Table 10. (Tables of bond angles for both phases are available from the authors upon request.) Like the M_{24} structure, the M_{14} structure is also based on a mixed cubic–hexagonal oxygen close-packing but with a shorter six-layer (c^2hc^2h) repeat along the *a* axis. The Ge atoms again occupy tetrahedral (Ge2 and Ge3) and octahedral (Ge1) sites while the Co and Mg atoms are mixed on the octahedral sites only. The hexagonal (*h*) layers at $x = \pm 1/4$ are, in this case, associated with the *b* glide planes of the *Pbam* space group and also lead to the formation of (100) olivine-type slabs containing the *M*3, *M*4, *M*6, Ge2, and Ge3 sites (cf. Fig. 3).

As shown in Table 6, a strong Co/Mg partitioning is also observed among the octahedral sites of the M_{14} structure with Co contents varying from 26% in the *M*3 site to 90% in the *M*2 site, for an overall composition of 52% Co. Like in the M_{24} structure, the Co atoms show a strong preference for the *M*2 site sharing two opposite edges with the $Ge1O_6$ octahedron (cf. Fig. 3) but the absence of correlation between the site populations and the average *M*–O bond distances is again noteworthy (cf. Table 11). Interestingly, very similar trends in cation ordering are also found in the $(Ni, Mg)_{14}Ge_5O_{24}$ structure and the high-pressure $(Fe, Mg)_{14}Si_5O_{24}$ structure (9), even though their overall transition-metal contents are quite different (cf. Table 11). In particular, the preference of the divalent transition cations for the octahedral *M*2 site is clearly seen in all three *M*14 structures, increasing in the order $Co^{2+} < Ni^{2+} < Fe^{2+}$. It appears that this effect could be a consequence of a particularly strong crystal field associated with the geometry of the *M*2 site: as illustrated in Fig. 4, its 2/*m* point symmetry corresponds to a strong equatorial distortion (with two short edges of 2.70 Å shared with GeO_6 octahedra and two much longer unshared edges of 3.31 Å) while maintaining a very narrow spread of the *M*2–O bond lengths (with a

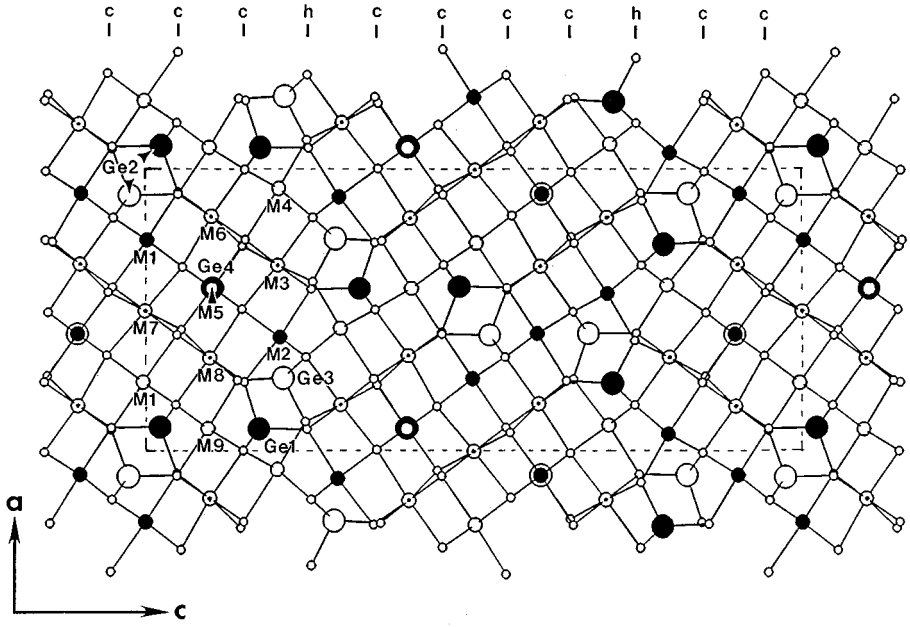

FIG. 2. Projection of the $(Co, Mg)_{24}Ge_8O_{40}$ structure on the (010) plane. Large, medium and small circles represent Ge, (Co,Mg), and O atoms, respectively. The heights of the Ge and metal atoms are indicated as follows: filled, open, and dotted circles represent approximate heights of 1/4, 3/4, and (0 and 1/2), respectively. The structure is based on a ten-layer (c^4hc^4h) close-packing along the c direction. The h layers correspond to the formation of mixed octahedral–tetrahedral olivine-type double layers. Note that the $M5$ and $M7$ octahedra share two opposite edges with the Ge4 octahedron.

standard deviation of 0.007 Å only). As shown in Table 11, a good correlation is actually observed between the populations of the octahedral sites of the M_{14} structure and their regularity (as measured by the standard deviations, σ, of the M–O bond distances): the transition-metal content of the individual M sites decreases fairly steadily with increasing values of σ. Although the origin of this correlation is unclear at the moment, it is noteworthy that it also applies to the Co/Mg ordering in the $(Co, Mg)_{24}Ge_8O_{40}$ structure (cf. Tables 5 and 8) and to the Ni/Mg ordering in the $(Ni, Mg)_{10}Ge_3O_{16}$ structure (4).

THE $M_{10n-2}Ge_{3n+1}O_{16n}$ STRUCTURAL FAMILY

The structure determinations of the M_{24} and M_{14} phases described above establish that they are based on the same building principle of periodic (glide-reflection) twinning of a parent cubic close-packed structure. As illustrated in Fig. 5, this parent structure actually corresponds to the $M_{10}Ge_3O_{16}$ phase which has been described previously in the cases of the $(Ni, Mg)_{10}Ge_3O_{16}$ and $Co_{10}Ge_3O_{16}$ compounds (4, 5, 10). This cubic close-packed structure is closely related to the spinel structure type, consisting of a regular intergrowth of triple $\{111\}$ spinel layers and single $\{111\}$ rock-salt layers (Fig. 5a). The insertion of periodic glide planes parallel to the (011) plane of its rhombohedral unit cell generates the M_{24} and M_{14} structures as follows: a glide operation on every fifth (011) plane (i.e., $n = 5$) results in the (c^4h) layer sequence of the M_{24} structure, the unit cell of which contains two twin slabs of identical width (5,5) and is, therefore, orthorhombic (Fig. 5b); similarly, a glide operation on every third (011) plane (i.e., $n = 3$) yields the (c^2h) layer sequence of the M_{14} structure with a (3, 3) orthorhombic unit cell (Fig. 5c). Other twinning periodicities are obviously possible, leading to other members of the structural family (cf. below). However, since the glide operation must generate olivine-type double layers, it can only occur on the mixed octahedral–tetrahedral layers of the parent M_{10} structure and, consequently, only odd values of n are allowed. As shown in Fig. 5d, the $n = 1$ end member of the structural family corresponds to the olivine structure itself with a simple (h) layer sequence.

As expected in a structural series based on the building principle of unit-cell twinning (13), microscopic intergrowths of the $M_{10n-2}Ge_{3n+1}O_{16n}$ phases readily occur, their formation being further facilitated by the proximity of their chemical compositions (cf. Fig. 1). An image of a highly disordered intergrowth observed by transmission electron microscopy in a multiphase sample in the NiO–MgO–GeO_2 system is shown in Fig. 6. The intuitive interpretation of the image contrast allows one to recognize the glide-reflection twinning operation and regions containing twin blocks of various widths. Apart from the known M_{10} ($n = \infty$, untwinned), M_{24} (5, 5), and M_{14} (3, 3) phases which are easily identified by their periodicities, the image also shows a narrow region with an unsymmetrical (5, 3) twin

TABLE 8
Selected Bond Lengths (Å) for the $(Co, Mg)_{24}Ge_8O_{40}$ Structure

Ge(1)–O(13)		1.771(3)	M(4)–O(10)		2.003(3)
Ge(1)–O(1)		1.771(3)	M(4)–O(2) #14	(×2)	2.079(2)
Ge(1)–O(2)	(×2)	1.772(2)	M(4)–O(5) #16	(×2)	2.117(2)
			M(4)–O(9) #3		2.231(3)
Ge(2)–O(4)	(×2)	1.765(2)	⟨M(4)–O⟩		2.104
Ge(2)–O(3)		1.771(3)			
Ge(2)–O(14)		1.777(3)	M(5)–O(15) #1	(×2)	2.121(2)
			M(5)–O(6) #1	(×2)	2.127(2)
Ge(3)–O(7)		1.715(3)	M(5)–O(9)		2.128(3)
Ge(3)–O(5)	(×2)	1.748(2)	M(5)–O(11) #20		2.147(3)
Ge(3)–O(10) #3		1.762(3)	⟨M(5)–O⟩		2.128
Ge(4)–O(6)	(×2)	1.879(2)	M(6)–O(2)		2.077(2)
Ge(4)–O(15)	(×2)	1.891(2)	M(6)–O(14) #3		2.097(2)
Ge(4)–O(8)		1.896(3)	M(6)–O(3) #9		2.098(2)
Ge(4)–O(12)		1.898(3)	M(6)–O(15)		2.102(2)
			M(6)–O(9) #		2.120(2)
M(1)–O(14) #3		2.067(3)	M(6)–O(8)		2.126(2)
M(1)–O(4) #2	(×2)	2.092(2)	⟨M(6)–O⟩		2.103
M(1)–O(15)	(×2)	2.107(2)			
M(1)–O(11)		2.134(3)	M(7)–O(11)	(×2)	2.090(2)
⟨M(1)–O⟩		2.100	M(7)–O(12)	(×2)	2.113(2)
			M(7)–O(15)	(×2)	2.137(2)
M(2)–O(5) #2	(×2)	2.026(2)	⟨M(7)–O⟩		2.113
M(2)–O(1) #10		2.092(3)			
M(2)–O(13)		2.108(3)	M(8)–O(7) #9		2.021(2)
M(2)–O(6) #11	(×2)	2.200(2)	M(8)–O(12) #12		2.051(2)
⟨M(2)–O⟩		2.109	M(8)–O(4) #3		2.076(2)
			M(8)–O(13)		2.092(2)
M(3)–O(10) #14		2.079(2)	M(8)–O(6) #12		2.134(2)
M(3)–O(8) #10		2.089(2)	M(8)–O(11) #14		2.142(2)
M(3)–O(1)		2.100(2)	⟨M(8)–O⟩		2.086
M(3)–O(6) #10		2.120(2)			
M(3)–O(5) #9		2.135(2)	M(9)–O(3)		2.025(3)
M(3)–O(9) #19		2.152(2)	M(9)–O(7)		2.044(3)
⟨M(3)–O⟩		2.112	M(9)–O(4) #26	(×2)	2.108(2)
			M(9)–O(2) #1	(×2)	2.137(2)
			⟨M(9)–O⟩		2.093

Symmetry transformations used to generate equivalent atoms:

#1	$x, -y+1/2, z$	#2	$x, -y+3/2, z$	#3	$-x+1, -y+1, -z+1$
#4	$-x+3/2, -y+1, z-1/2$	#5	$x, y+1, z$	#6 $x-1, y, z$	
#7	$x-1, -y+1/2, z$	#8	$x-1/2, y, -z+1/2$	#9	$x, y-1, z$
#10	$x+1/2, y, -z+1/2$	#11	$x+1, -y+1/2, z$	#12	$x+1, y, z$
#13	$x+1/2, -y+1/2, -z+1/2$	#14	$-x+1, -y, -z+1$	#15	$-x+1, y+1/2, -z+1$
#16	$-x+3/2, y-1/2, z+1/2$	#17	$-x+3/2, -y+1, z+1/2$	#18	$-x+3/2, y+1/2, z+1/2$
#19	$x+1/2, y-1, -z+1/2$	#20	$-x, -y+1, -z+1$	#21	$x-1/2, -y+1/2, -z+1/2$
#22	$x-1/2, y+1, -z+1/2$	#23	$-x, -y, -z+1$	#24	$-x, y-1/2, -z+1$
#25	$-x, y+1/2, -z+1$	#26	$-x+1, -y+2, -z+1$	#27	$-x+1, y-1/2, -z+1$

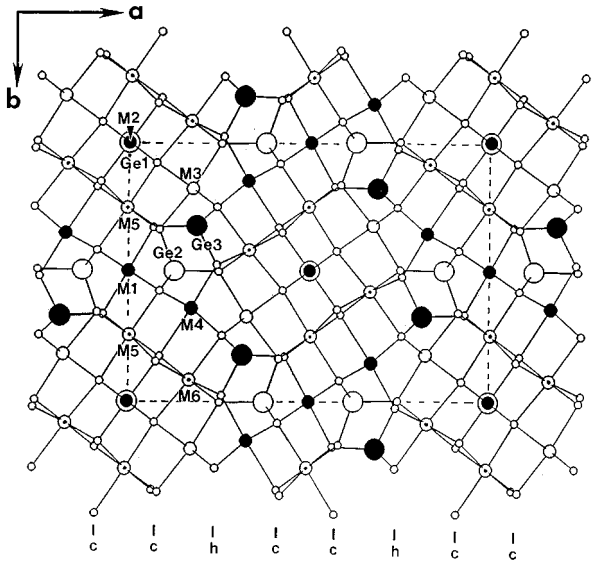

FIG. 3. Projection of the $(Co, Mg)_{14}Ge_5O_{24}$ structure on the (001) plane. Large, medium, and small circles represent Ge, (Co, Mg), and O atoms, respectively. The heights of the Ge and metal atoms are indicated as follows: filled, open, and dotted circles represent approximate heights of 1/2, 0, and (1/4 and 3/4), respectively. The structure is based on a six-layer (c^2hc^2h) close-packing along the *a* direction. The *h* layers correspond to the formation of mixed octahedral–tetrahedral olivine-type double layers. Note that the *M*2 octahedron shares two opposite edges with the Ge1 octahedron (cf. Fig. 4).

sequence and monoclinic symmetry. This phase can be regarded as a new member of the $M_{10n-2}Ge_{3n+1}O_{16n}$ family resulting from the intergrowth of the M_{24} and M_{14} phases, i.e., $M_{38}Ge_{13}O_{64}$ (corresponding to the "forbidden" value of 4 for the *n* index). In spite of the moderate image resolution, it is clear that intergrowth occurs without any defects at the phase boundaries as can be expected from the very close structural similarities among the various phases.

CONCLUSION

The structure determinations of the $(M, Mg)_{24}Ge_8O_{40}$ and $(M, Mg)_{14}Ge_5O_{24}$ (M = Co, Ni) compounds have led to the elucidation of the building principle and the correct formulation of the $M_{10n-2}Ge_{3n+1}O_{16n}$ structural family. The members $n = \infty$, 5, 3, and 1 form as stable phases in the CoO–MgO–GeO_2 system (this study), as well as in the NiO–MgO–GeO_2 system (Ref. 6, although, in this earlier work, the structural series had been wrongly formulated as $M_{4n+6}Ge_{2n+1}O_{8(n+1)}$). Based on the similarity of the phase diagram reported for the FeO–MgO–GeO_2 system (14), the same phases may exist in that system as well. All phases of the $M_{10n-2}Ge_{3n+1}O_{16n}$ structural family (except the $n = 1$ olivine end member) contain octahedrally coordinated Ge

TABLE 9
Selected Bond Lengths (Å) for the $(Co, Mg)_{14}Ge_5O_{24}$ Structure

Ge(1)–O(7)	(×4)	1.890(1)	*M*(4)–O(6)		2.007(2)
Ge(1)–O(2) #4	(×2)	1.909(2)	*M*(4)–O(8)	(×2)	2.081(2)
			M(4)–O(9)	(×2)	2.111(2)
Ge(2)–O(8) #6	(×2)	1.772(1)	*M*(4)–O(5)		2.249(2)
Ge(2)–O(3) #7		1.774(2)			
Ge(2)–O(1)		1.776(2)	*M*(5)–O(4)		2.0310(14)
			M(5)–O(2) #5		2.067(2)
Ge(3)–O(4)		1.715(2)	*M*(5)–O(8) #5		2.083(2)
Ge(3)–O(9)	(×2)	1.749(2)	*M*(5)–O(1)		2.118(2)
Ge(3)–O(6) #9		1.763(2)	*M*(5)–O(7)		2.126(2)
			M(5)–O(5) #5		2.1307(14)
M(1)–O(4)	(×2)	1.998(2)			
M(1)–O(8) #5	(×4)	2.120(2)	*M*(6)–O(6) #9		2.0754(14)
			M(6)–O(3) #7		2.088(2)
M(2)–O(7)	(×4)	2.136(2)	*M*(6)–O(2)		2.096(2)
M(2)–O(5) #5	(×2)	2.151(2)	*M*(6)–O(5)		2.1272(14)
			M(6)–O(7) #6		2.130(2)
M(3)–O(9)	(×2)	2.032(2)	*M*(6)–O(9)		2.162(2)
M(3)–O(1)		2.102(2)			
M(3)–O(3)		2.104(2)			
M(3)–O(7)	(×2)	2.211(2)			

Symmetry transformations used to generate equivalent atoms:

#1	$-x, -y, -z$	#2	$x, y, -z$	#3	$-x, -y, z$
#4	$-x+1/2, y-1/2, -z$	#5	$x-1/2, -y+1/2, z$	#6	$-x+1/2, y+1/2, z$
#7	$-x+1/2, y+1/2, -z$	#8	$x, y, -z+1$	#9	$-x+1/2, y+1/2, -z+1$
#10	$-x, -y+1, -z+1$	#11	$x-1/2, -y+1/2, -z+1$	#12	$-x, -y, -z+1$
#13	$-x+1/2, y-1/2, -z+1$	#14	$-x+1/2, y-1/2, z$	#15	$x, y, z+1$
#16	$x+1/2, -y+1/2, -z+1$	#17	$x+1/2, -y+1/2, z$	#18	$x+1/2, -y+1/2, -z$

TABLE 10
Selected Bond Lengths (Å) for the $(Ni, Mg)_{14}Ge_5O_{24}$ Structure

Ge(1)–O(7)	(×4)	1.883(3)			
Ge(1)–O(2) #4	(×2)	1.908(4)	*M*(4)–O(6)		2.005(4)
			M(4)–O(8)	(×2)	2.074(3)
Ge(2)–O(8) #6	(×2)	1.764(3)	*M*(4)–O(9)	(×2)	2.090(3)
Ge(2)–O(1)		1.773(4)	*M*(4)–O(5)		2.250(4)
Ge(2)–O(3) #6		1.773(3)			
			M(5)–O(4)		2.011(3)
Ge(3)–O(4)		1.720(4)	*M*(5)–O(2) #4		2.049(3)
Ge(3)–O(9)	(×2)	1.743(3)	*M*(5)–O(8) #4		2.077(3)
Ge(3)–O(6) #9		1.760(4)	*M*(5)–O(1)		2.108(3)
			M(5)–O(5) #4		2.108(3)
M(1)–O(4)	(×2)	1.987(4)	*M*(5)–O(7)		2.112(3)
M(1)–O(8) #4	(×4)	2.111(3)			
			M(6)–O(6) #9		2.054(3)
M(2)–O(7)	(×4)	2.113(3)	*M*(6)–O(3) #6		2.074(3)
M(2)–O(5) #4	(×2)	2.125(4)	*M*(6)–O(2)		2.087(3)
			M(6)–O(7) #7		2.107(3)
			M(6)–O(5)		2.114(3)
M(3)–O(9)	(×2)	2.026(3)	*M*(6)–O(9)		2.134(3)
M(3)–O(3)		2.085(4)			
M(3)–O(1)		2.097(4)			
M(3)–O(7)	(×2)	2.222(3)			

Symmetry transformations used to generate equivalent atoms:

#1	$-x, -y, -z$	#2	$x, y, -z$	#3	$-x, -y, z$
#4	$-x+1/2, y-1/2, -z$	#5	$x-1/2, -y+1/2, z$	#6	$-x+1/2, y+1/2, z$
#7	$-x+1/2, y+1/2, -z$	#8	$x, y, -z+1$	#9	$-x+1/2, y+1/2, -z+1$
#10	$-x, -y+1, -z+1$	#11	$x-1/2, -y+1/2, -z+1$	#12	$-x, -y, -z+1$
#13	$-x+1/2, y-1/2, -z+1$	#14	$-x+1/2, y-1/2, z$	#15	$x, y, z+1$
#16	$x+1/2, -y+1/2, -z+1$	#17	$x+1/2, -y+1/2, z$	#18	$x+1/2, -y+1/2, -z$

atoms and silicate analogs of the M_{10} and M_{24} phases may therefore also be expected to form at high pressures, as has already been found for the $M_{14}Si_5O_{24}$ phase (7–9).

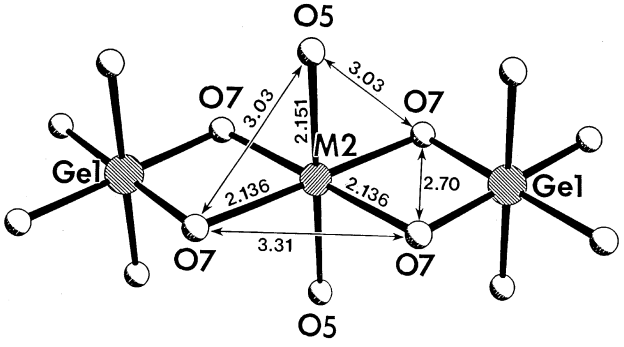

FIG. 4. Coordination geometry around the *M*2 octahedral site of the $(Co, Mg)_{14}Ge_5O_{24}$ structure (distances in Å). The *M*2 site symmetry is $2/m$ with the 2-fold axis parallel to the Ge1–*M*2–Ge1 row and the *c* axis of the M_{14} unit cell (cf. Fig. 3). Notice the strong equatorial distortion resulting from short O7–O7 edges shared with the Ge1 octahedra and much longer unshared O7–O7 edges (cf. Fig. 3).

TABLE 11
Populations, Average Bond Lengths, and Bond Length Standard Deviations for the Octahedral Sites in the $(Co, Mg)_{14}Ge_5O_{24}$ (52% Co), $(Ni, Mg)_{14}Ge_5O_{24}$ (21% Ni), and $(Fe, Mg)_{14}Si_5O_{24}$ (12% Fe) Phases

Octahedral site	*M*2	*M*6	*M*5	*M*1	*M*4	*M*3
%Co	90	67	52	34	38	26
⟨*M*–O⟩ (Å)	2.141	2.113	2.093	2.079	2.107	2.115
σ (Å)*	0.007	0.030	0.036	0.058	0.073	0.074
%Ni	58	27	24	16	10	2
⟨*M*–O⟩ (Å)	2.117	2.095	2.077	2.070	2.097	2.113
σ (Å)*	0.006	0.026	0.037	0.058	0.074	0.082
%Fe**	41	11	7	12	8	9
⟨*M*–O⟩ (Å)	2.135	2.102	2.086	2.121	2.100	2.115
σ (Å)*	0.007	0.030	0.036	0.058	0.073	0.074

* σ represents the standard deviation of the six *M*–O bond lengths for each MO_6 octahedron.

** The data for the $(Fe, Mg)_{14}Si_5O_{24}$ phase are from Hazen *et al.* (9).

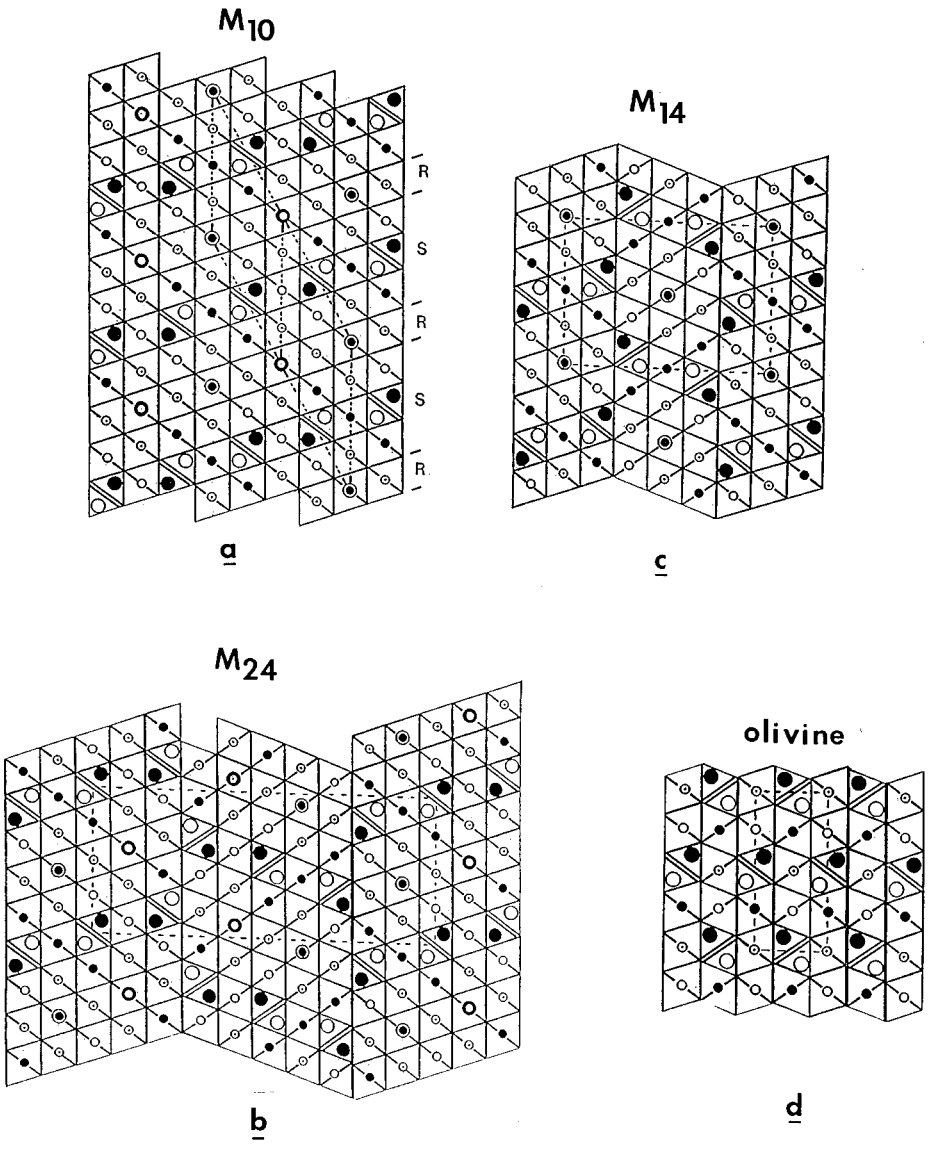

FIG. 5. Illustration of the "unit-cell twinning" building principle of the $M_{10n-2}Ge_{3n+1}O_{16n}$ structural family. Large and small circles represent Ge and M atoms, respectively; oxygen atoms at the corners of the polyhedra have been omitted. Filled, open and dotted circles represent the relative heights of atoms, e.g., approximately 0, 1/2 and $\pm 1/4$. The rhombohedral cubic close-packed M_{10} structure (the $n = \infty$ end member, in a) is built of alternating spinel (S) and rock-salt (R) layers. The orthorhombic M_{24} and M_{14} structures (the $n = 5$ and $n = 3$ members in b and c, respectively) are generated by the periodic insertion of glide planes in the M_{10} structure producing the (5, 5) and (3, 3) twin repeats. Note that the structures contain olivine-type double layers at the twin block boundaries. The (ideally) hexagonal close-packed olivine structure (in d) represents the $n = 1$ end member of the structural family.

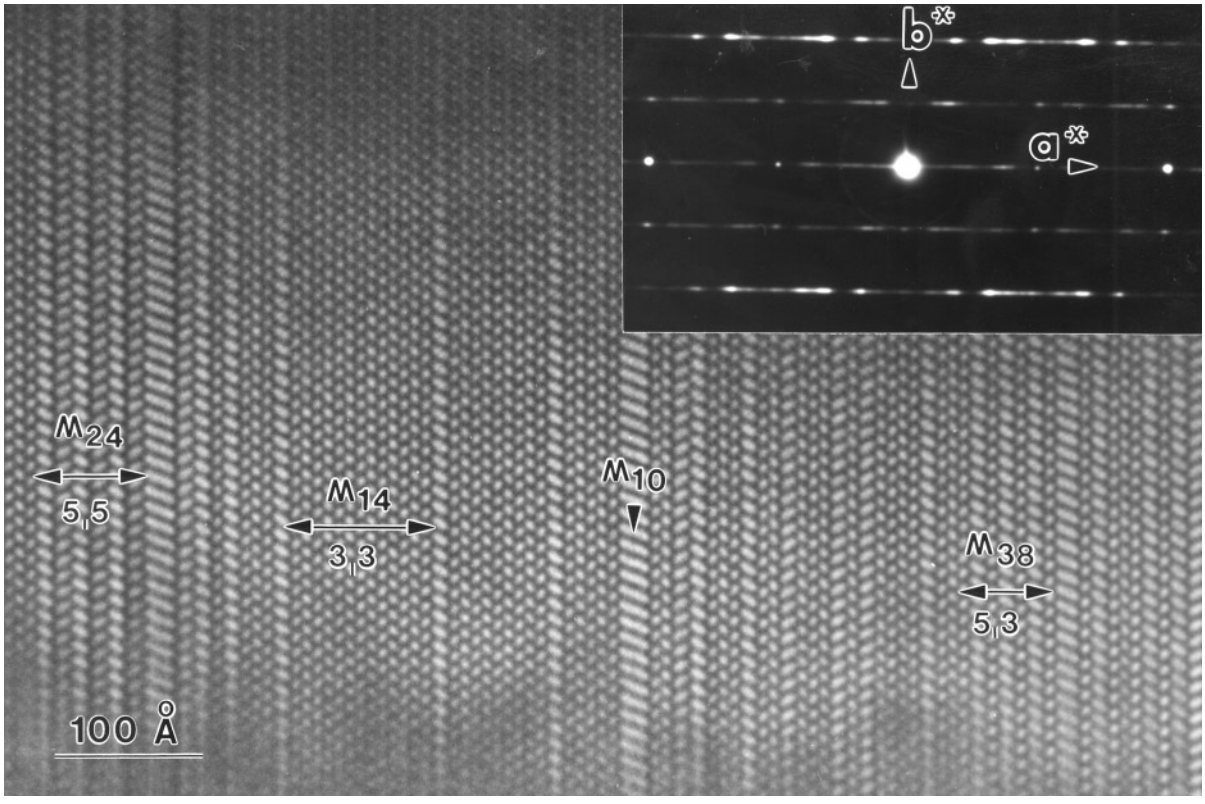

FIG. 6. Image by transmission electron microscopy of an intergrowth of $M_{10n-2}Ge_{3n+1}O_{16n}$ phases in the NiO–MgO–GeO_2 system. The high degree of disorder in the image is also shown by the pronounced streaking in the diffraction pattern (axis labels referring to the M_{14} unit cell). Regions corresponding to the M_{10}, M_{24} and M_{14} phases are easily recognized from their twin sequences and periodicities by comparison with the structural models in Fig. 5. A narrow slab of a new M_{38} phase is also visible, corresponding to a mixed (5, 3) twin sequence and the (formally) $n = 4$ member of the structural family.

ACKNOWLEDGMENTS

This work was supported by a research grant from the Canadian Natural Sciences & Engineering Research Council (NSERC). The single-crystal X-ray intensity data were collected by Dr. J. Britten of McMaster University.

REFERENCES

1. A. Navrotsky, *J. Solid State Chem.* **6,** 21 (1973).
2. R. B. Von Dreele, P. W. Bless, E. Kostiner, and R. E. Hughes, *J. Solid State Chem.* **2,** 612 (1970)
3. J. Barbier, *J. Solid State Chem.* **68,** 52 (1987).
4. M. E. Fleet and J. Barbier, *Acta Crystallogr. C* **44,** 232 (1988).
5. M. E. Fleet and J. Barbier, *Acta Crystallogr. B* **45,** 201 (1989).
6. J. Barbier, *Acta Crystallogr. B* **43,** 422 (1987).
7. L. W. Finger, J. Ko, R. M. Hazen, T. Gasparik, R. J. Hemley, C. T. Prewitt, and D. J. Weidner, *Nature* **341,** 140 (1989).
8. L. W. Finger, R. M. Hazen, and C. T. Prewitt, *Am. Mineral.* **76,** 1 (1991).
9. R. M. Hazen, L. W. Finger, and J. Ko, *Am. Mineral.* **77,** 217 (1992).
10. J. Barbier, *Acta Crystallogr. C* **51,** 343 (1995).
11. G. M. Sheldrick, "SHELXL, Program for the refinement of Crystal Structures," University of Göttingen, Germany, 1993.
12. G. M. Sheldrick, *Acta Crystallogr. A* **46,** 467 (1990).
13. B. G. Hyde, S. Andersson, M. Bakker, C. M. Plug, and M. O'Keeffe, *Prog. Solid State Chem.* **12,** 273 (1979).
14. A. Navrotsky and L. Hughes, *J. Solid State Chem.* **16,** 185 (1976).